Constraining Gravitino Dark Matter with the Cosmic Microwave Background

Raphael Lamon
Institut für Theoretische Physik, ETH Zürich, Hönggerberg, 8093 Zürich, Switzerland.

Ruth Durrer
Département de Physique Théorique, Université de Genève, 24 quai Ernest Ansermet, 1211 Genève 4, Switzerland.

(Dated: January 20, 2006)

We consider super-gravity models in which the lightest supersymmetric particle (LSP) is a stable gravitino. The next-to-lightest supersymmetric particle (NLSP) freezes out with its thermal relic density and then decays after $(10^5 - 10^{10})$ sec, injecting high-energy photons into the cosmic plasma. These photons heat up the electron plasma which then thermalizes with the cosmic microwave background (CMB) via Compton scattering, bremsstrahlung and double-Compton scattering. Contrary to previous studies which assume instantaneous energy injection, we solve the full kinetic equation for the photon number density with a source term describing the decay of the NLSP. This source term is based on the requirement that the injected energy be almost instantaneously redistributed by Compton scattering, hence leading to a time-dependent chemical potential. We investigate the case of a stau NLSP and determine the constraints on the gravitino and stau masses from observations of the CMB spectrum by assuming that all gravitino LSPs come from stau NLSP decays. Unlike the analytical approximations, we find that there may be a stau mass below which the constraint from the CMB spectrum vanishes.

PACS numbers: 95.35.+d, 98.80.Es, 98.80.Cq

I. INTRODUCTION

Supersymmetry provides mainly two compelling candidates for cold dark matter: either the gravitino or the neutralino, depending on which one is the LSP. If we require that R-parity be conserved, the NLSP decays into the stable LSP and releases energy in standard model particles. At leading order, these late decays are two-body and the accompanying energy is mainly electromagnetic.

Part of the electromagnetic release is transferred to the cosmic microwave background radiation. The CMB then re-thermalizes through three relevant processes: Compton scattering ($\gamma+e \to \gamma+e$), double-Compton scattering ($\gamma+e \to \gamma+\gamma+e$) and bremsstrahlung ($e+p \to e+p+\gamma$). The energy injection may distort the CMB, depending on the redshift at which it occurs and on the various time scales of the processes. Early NLSP decays can be fully thermalized, whereas distortions caused by injection from late decays cannot. Varying the NLSP and LSP masses, it is possible to control both the NLSP lifetime and the energy injected in the CMB.

The CMB is not only very isotropic, but it also has a very precise Planck spectrum. The FIRAS instrument aboard the COBE satellite constrains the deviation from a perfect blackbody spectrum in terms of a few numbers. Important for this work is the limit for the chemical potential [1]

$$|\mu| \leq 9 \times 10^{-5} \ .$$

This bound has been used to derive limits for the energy released by NLSP decays as well as the NLSP lifetime. Observational constraints on the CMB spectrum can be translated into bounds for the stau NLSP and gravitino LSP masses. It should be mentioned that we explicitly assume that all gravitinos present in the universe are produced by stau decays. Some models suggest that gravitino LSPs may also be produced by scattering interactions after reheating, leading to less stringent constraints. Recently, several papers have employed an analytic approximation to determine these limits [2–4]. The approximation used in [2–4] is derived in Ref. [5]. This analytical result turns out to provide the most stringent limit on the gravitino dark matter model in some range for the NLSP and LSP masses. This prompted us to repeat the calculation numerically.

We find that the bounds for a chemical potential of $\mu < 9\times10^{-5}$ given by [5] is a good approximation only for stau masses above 500 GeV. Below this mass, our bounds are less stringent and even disappear for staus lighter than 100 GeV. We also consider the limit $\mu < 10^{-5}$ and find that our results suggest lighter gravitinos or equivalently shorter stau lifetimes. Finally, we consider an upper bound on the chemical potential of 2×10^{-6} as planned to be achieved in the DIMES experiment [6]. We find that, if DIMES does not see a chemical potential, $\mu < 2 \times 10^{-6}$, gravitinos cannot significantly contribute to the dark matter if supersymmetry breaking is gravity mediated.

After recalling some properties of the NLSP in the next section, we write down the full kinetic equation for the evolution of the photon one-particle distribution function in Section III. We express it as an evolution equation for a frequency-dependent chemical potential. This allows us to determine the chemical potential for a given point

in the $(m_{\rm NLSP}, m_{\rm LSP})$ and $(m_{\rm NLSP}, \tau_{\rm NLSP})$ plane of the NLSP and to draw exclusion plots in Section IV. We summarize our conclusions in Section V.

II. NLSP PROPERTIES

We investigate a super-gravity model with a gravitino LSP and a stau NLSP. We assume that the NLSP freezes out with thermal relic density and decays after a time determined by both its mass and the LSP mass. Due to the suppression of non-photonic decay channels, the branching ratio for decays to photons is set to be equal to one.

Gravitino LSPs are produced through NLSP decays NLSP $\rightarrow$ LSP + SMP, where SMP are standard model particles. Using the standard $N = 1$ super-gravity Lagrangian, the rates for the various decay channels of the NLSP can be calculated.

A. Slepton NLSP

We assume a gravity-mediated supersymmetry breaking model, where the gravitino LSP mass is of the order $10^2 - 10^4$ GeV and the stau NLSP lifetime of the order $10^4 - 10^{10}$ sec. In gauge-mediated supersymmetry breaking models the gravitino is also the LSP but is much lighter ($m_{\tilde{G}} \lesssim$ keV), resulting in a much shorter NLSP lifetime. In such models, the present CMB constraints do therefore not apply.

The width for the decay of any sfermion $\tilde{f}$ to a gravitino $\tilde{G}$ for a negligible fermion mass is given by

$$\Gamma(\tilde{f} \rightarrow f\tilde{G}) = \frac{1}{48\pi M_*^2}\frac{m_{\tilde{f}}^5}{m_{\tilde{G}}^2}\left[1 - \frac{m_{\tilde{G}}^2}{m_{\tilde{f}}^2}\right]^4, \qquad (1)$$

where $M_* = (8\pi G_N)^{-1/2}$ is the reduced Planck mass.

Stau NLSPs decay to taus and gravitinos, which then decay to e, μ, π^0, $\pi^\pm$ and ν. As mentioned in Ref. [3], the electromagnetic energy produced in τ decays varies between $\epsilon_{\rm EM}^{\rm min} \approx \frac{1}{3}E_\tau$ and $\epsilon_{\rm EM}^{\rm max} = E_\tau$. If not specified, a value of $\epsilon_{\rm EM} = 0.8E_\tau$ will be assumed throughout of this paper.

B. Thermal relic density

Using the thermal relic density of the right-handed slepton NLSPs determined in Ref. [7] and the thermally-averaged cross section from Ref. [8], the stau relic abundance is given by

$$\Omega_{\tilde{\tau}}^{\rm th}h^2 \approx 0.2\left[\frac{m_{\tilde{\tau}}}{\rm TeV}\right]^2. \qquad (2)$$

As long as the staus do not decay, their time-dependent number density can be expressed as

$$n_{\tilde{\tau}}(t) \approx 0.26\ {\rm m}^{-3}\left[\frac{\rm GeV}{m_{\tilde{\tau}}}\right]\left[\frac{T}{\rm Kelvin}\right]^3\Omega_{\tilde{\tau}}. \qquad (3)$$

The fact that the final gravitino density, $\Omega_{\tilde{G}}h^2 = (m_{\tilde{G}}/m_{\tilde{\tau}})\Omega_{\tilde{\tau}}h^2$, is bounded by observations, $\Omega_{\tilde{G}}h^2 \leq 0.14$ [9] together with Eq. (2) implies an upper bound for the gravitino mass as a function of the stau mass:

$$\frac{m_{\tilde{G}}}{\rm GeV} < 0.7 \times 10^6\frac{\rm GeV}{m_{\tilde{\tau}}}. \qquad (4)$$

III. EVOLUTION EQUATION FOR THE PHOTON NUMBER DENSITY

The decay of unstable particles into photons during the early stages of the universe can lead to distortions in the CMB. Depending on the redshift at which energy is injected, this may leave a measurable imprint of the early decays. This is the process which we now analyze in detail.

A. Energy injection by particle decays

Energy injection resulting from NLSP decays heats the electrons, leading to a ratio $T_e/T_{\rm CMB}$ larger than one, where T_e is the electron temperature and $T_{\rm CMB}$ is the temperature of the CMB. Due to the tight coupling between electrons and photons during the early stages of the universe, the energy surplus of the electrons is redistributed among the photons, distorting the CMB photon distribution from a blackbody spectrum. Assuming that the energy transfer between electrons and photons results in a Bose-Einstein spectrum with a frequency-independent chemical potential, it is possible to relate this resulting chemical potential to the number and energy density of the injected photons and electrons.

Following the analysis done in [5], we can write the energy in a Bose-Einstein distribution as

$$\rho_{\rm BE} = 4\sigma_{SB}T_e^4\left(1 - \frac{90\zeta(3)}{\pi^4}\mu_{\rm inj}\right), \qquad (5)$$

where we assume a small chemical potential. The number density is given by

$$n_{\rm BE} = \frac{2\zeta(3)}{\pi^2}T_e^3\left(1 - \frac{\pi^2}{6\zeta(3)}\mu_{\rm inj}\right). \qquad (6)$$

Here ζ denotes the Riemann ζ-function (see Ref. [10]). Furthermore, due to energy conservation, we know that the energy density may also be written as

$$\rho_{\rm BE} = \rho_{\rm P} + \rho_{\rm decay}, \qquad (7)$$

where $\rho_{\rm decay}$ is the energy density injected by the NLSP decays and ρ_P is the density of the CMB photons. This

equation is only valid if the injected photons are redistributed in a negligible amount of time compared to the time scales of double-Compton and bremsstrahlung. However, this does not hold for the low-frequency spectrum, where the photon-creating processes dominate.

More precisely, the injected energy density is given by the following differential equation

$$\frac{d\rho_{\rm decay}}{dt} = \epsilon \frac{m_{\rm NLSP}^2 - m_{\rm LSP}^2}{2m_{\rm NLSP}} n_{\rm NLSP}(t) \frac{e^{-t/\tau}}{\tau} - 4\frac{\dot{a}}{a}\rho_{\rm decay}, \tag{8}$$

where τ is the lifetime of the NLSP. Due to the fact that tau decays also produce several neutrinos, the right hand side of Eq. (8) has been multiplied by a factor ϵ describing the ratio of the injected energy to the total energy. As pointed out in Sec. II A, ϵ may have a value between 0.3 and 1; we set $\epsilon = 0.8$. In order to solve Eq. (8), we integrate both sides from $t_{\rm in}$ to t and obtain

$$\begin{aligned}\rho_{\rm decay} &= \epsilon \frac{m_{\rm NLSP}^2 - m_{\rm LSP}^2}{2m_{\rm NLSP}} n_{\rm NLSP}(t_{\rm in}) \left(\frac{a_{\rm in}}{a}\right)^4 \\ &\times \left\{ \frac{1}{2}\sqrt{\pi}\left[{\rm Erf}\left(\sqrt{t/\tau}\right) - {\rm Erf}\left(\sqrt{t_{\rm in}/\tau}\right)\right] \right. \\ &\left. - \left[\sqrt{\frac{t}{t_{\rm in}}} e^{-t/\tau} - e^{-t_{\rm in}/\tau}\right]\right\}, \end{aligned} \tag{9}$$

where Erf is the error function as defined in [10]. Similarly, the photon number density is given by

$$n_{\rm BE} = n_{\rm P} + n_{\rm decay}, \tag{10}$$

where $n_{\rm decay}$ is the injected photon number density given by the following differential equation

$$\frac{dn_{\rm decay}}{dt} = N_\gamma n_{\rm NLSP}(t) \frac{e^{-t/\tau}}{\tau} - 3\frac{\dot{a}}{a} n_{\rm decay}. \tag{11}$$

Here N_γ is the number of photons per stau decay injected into the spectrum. The solution of Eq. (11) is given by

$$n_{\rm decay} = N_\gamma n_{\rm NLSP}(t_{\rm in}) \left(\frac{a_{\rm in}}{a}\right)^3 \left(1 - e^{-t/\tau}\right). \tag{12}$$

Inserting Eq. (9) and Eq. (7) into Eq. (5), as well inserting (12) and Eq. (10) into Eq. (6) we find the relations:

$$\begin{aligned} 1 + \frac{n_{\rm decay}}{n_{\rm P}} &= \left(\frac{T_e}{T}\right)^3 \left(1 - \frac{\pi^2}{6\zeta(3)}\mu_{\rm inj}\right) \\ 1 + \frac{\rho_{\rm decay}}{\rho_{\rm P}} &= \left(\frac{T_e}{T}\right)^4 \left(1 - \frac{90\zeta(3)}{\pi^4}\mu_{\rm inj}\right). \end{aligned} \tag{13}$$

These equations cannot be solved simultaneously since there are three unknowns, $\mu_{\rm inj}$, T_e and N_γ. However, it turns out that the chemical potential is independent of N_γ up to an unreasonable photon number injection of $\approx 10^7$ photons per NLSP decay, as shown in the bottom panel of Fig. 1. The top panel shows the time evolution of the chemical potential for two different stau lifetimes.

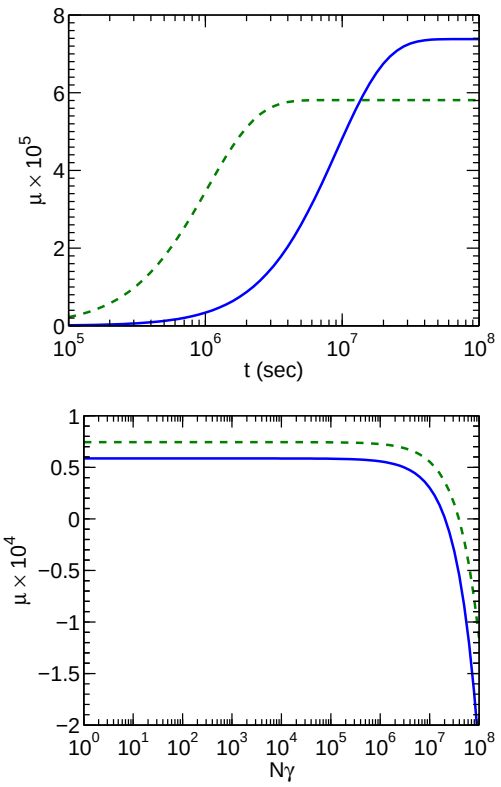

FIG. 1: Solution of the system of equations (13). Top: Time evolution of the chemical potential for fixed N_γ at $m_{\tilde{\tau}} = 200$ GeV and $m_{\tilde{G}} = 50$ GeV, corresponding to $\tau_{\rm NLSP} \approx 6\times10^6$ sec (blue solid line) and $m_{\tilde{\tau}} = 300$ GeV and $m_{\tilde{G}} = 50$ GeV, corresponding to $\tau_{\rm NLSP} \approx 7\times10^5$ sec (green dashed line). A value of $N_\gamma = 10^4$ has been assumed. Bottom: The chemical potential at a time $t = 10^8$ sec is shown as a function of N_γ. Both lines are given by the same masses as above.

Up to now, we have assumed that the energy injection caused by stau decays was instantaneously converted in a chemical potential through Compton scattering. However, there are also two other processes that do not conserve the photon numbers: bremsstrahlung and double-Compton scattering. The influence of both processes is discussed in the next section.

We shall use the value $\mu_{\rm inj}$ obtained in this section as initial condition for the numerical solution of the Boltzmann equation discussed below.

B. Photon-matter interaction

When the universe is more than a few minutes old, the coupling of CMB photons and matter is basically due to three processes: Compton scattering, double Compton scattering and bremsstrahlung. If these processes are no longer very efficient, the spectrum can be distorted. Especially, if double Compton scattering and bremsstrahlung become weak, the photon number can

no longer be changed and energy injection into the CMB leads to a chemical potential. With this in mind, we parameterize a general distorted spectrum by a Bose-Einstein distribution with a frequency-dependent dimensionless chemical potential $\mu(x,t)$,

$$n(x,t) = \frac{1}{\exp(x+\mu(x,t))-1}, \tag{14}$$

where $x = h\nu/T_e$ is the dimensionless photon frequency. The collision terms in the Boltzmann equation for the three relevant processes (Compton scattering, double-Compton scattering and bremsstrahlung) are studied in [11]. The Boltzmann equation is given by

$$\begin{aligned}\frac{\partial n}{\partial t} = & \frac{1}{t_{\gamma e}}\frac{T_e}{m_e}\frac{1}{x^2}\frac{\partial}{\partial x}\left(\frac{\partial n}{\partial x}+n+n^2\right) \\ & +\frac{Qg(x)}{t_{\gamma e}}\frac{1}{e^x x^3}\left[1-n\left(e^x-1\right)\right] \\ & +\left[1-\theta(x-1)\right]\frac{1}{t_{\gamma e}}\frac{4\alpha}{3\pi}\left(\frac{T_e}{m_e}\right)^2\frac{1}{x^3} \\ & \times\left[1-n\left(e^x-1\right)\right]\int dx x^4(1+n)n \\ & -\frac{e^{x+\mu_{\rm inj}}}{\left(e^{x+\mu_{\rm inj}}-1\right)^2}\frac{d\mu_{\rm inj}}{dt}. \end{aligned} \tag{15}$$

The first term describes Compton scattering, the second bremsstrahlung, the third term double Compton scattering and the fourth is the injection term given by the solution of Eq. (13). We have introduced the Heaviside function θ in the double-Compton scattering term, to take into account that it is active only for $x < 1$. The constant $t_{\gamma e} = (n_e\sigma_T)^{-1}$ is the Thomson scattering time, $Q = 2\sqrt{2\pi}(m_e/T_e)^{1/2}\alpha n_B T_e^{-3} \simeq 1.7\times10^{-10}({\rm MeV}/T)^{1/2}(T/T_e)^{7/2}\Omega_B h^2$ and $g(x)$ is the Gaunt factor. More details on the collision terms can be found in Refs. [5, 11] or [12].

Since we expect a small value of the chemical potential, we can expand this equation to first order in μ.

$$\begin{aligned} n(x,t) &\approx n_0(x,t)+\mu(x,t)\frac{\partial n_0}{\partial\mu}(x,t) \\ &= \frac{1}{e^x-1}-\mu(x,t)\frac{e^x}{(e^x-1)^2}. \end{aligned} \tag{16}$$

The zeroth order is the equilibrium distribution, and the first order in μ describes the spectral distortion. The kinetic equations for the three relevant processes (Compton scattering, double Compton scattering and bremsstrahlung) [11], then becomes a linear equation for the evolution of the chemical potential ($\mu' = \partial\mu/\partial x$),

$$\begin{aligned} -\frac{e^x}{(e^x-1)^2}\frac{\partial}{\partial t}\mu(x,t) = & \frac{2}{t_{\gamma e}}\frac{T_e}{m_e}\frac{xe^{2x}}{(e^x-1)^4}\times \\ & \left[(4-4\cosh x+x\sinh x)\mu'(x,t)\ -x(\cosh x-1)\mu''(x,t)\right] \\ & +\frac{Qg(x)}{t_{\gamma e}}\frac{1}{x^3(e^x-1)}\mu(x,t) \\ & +\left[1-\theta(x-1)\right]\frac{1}{t_{\gamma e}}\frac{16\pi^3\alpha}{45}\left(\frac{T_e}{m_e}\right)^2\frac{e^x}{x^3(e^x-1)}\mu(x,t) \\ & -\frac{e^x}{\left(e^x-1\right)^2}\frac{d\mu_{\rm inj}}{dt}. \end{aligned} \tag{17}$$

We have solved both systems of equations numerically and find consistent results. When interested in values $\mu \sim 10^{-5}$, we start at $t_{\rm in} = 10^5$ sec, but when we want to detect chemical potentials on the level of $\mu \sim 10^{-6}$ we have to start at $t_{\rm in} = 10^4$ sec.

C. Time evolution of the frequency-dependent chemical potential

As shown in Ref. [12], energy injected at a redshift higher than $z \sim 10^7$, corresponding to a time $t \lesssim 10^5$ sec is fully thermalized. Furthermore, at decoupling time $t_{\rm dec} \approx 10^{13}$ sec, the CMB spectrum is frozen in and does not evolve anymore apart from redshifting the photon momenta. However, as shown in Fig. 2, the photon-creating processes are unable to reduce a chemical potential already as early as $t \gtrsim 10^8$ sec, much before recombination.

We see from the top panel of Fig. 2 that, compared to the chemical potential of a Bose-Einstein spectrum (dashed blue line), double-Compton and bremsstrahlung significantly reduce the magnitude of the distortions from a blackbody spectrum: the chemical potential at late times has been reduced from 7.4×10^{-5} to 4.3×10^{-5}. The bottom panel of Fig. 2 shows the frequency dependence of μ evaluated at different times. The high-frequency range is dominated by Compton scattering. The chemical potential is constant above $x \gtrsim 1$, describing a true Bose-Einstein spectrum. The low-energy spectrum is dominated by the photon-creating processes which can destroy the chemical potential and lead to a Planck spectrum below $x \lesssim 4\times10^{-3}$ at recombination time.

It is clear that the later the energy injection, or equivalently the later the staus decay, the weaker are the photon-creating processes which would reduce the distortions. However, it should be kept in mind that our equations are valid only if Compton scattering can achieve a Bose-Einstein spectrum. By requiring that Compton scattering be well active during stau decays, we can put an upper limit on the stau lifetime. Following the analysis of [12], a given spectrum can only relax to a Bose-Einstein spectrum before $t_{\rm BE} \simeq 10^9$ sec. Therefore, the

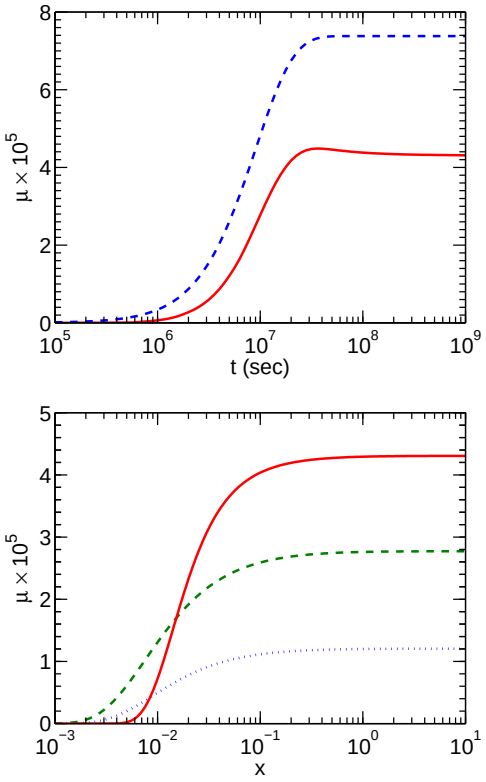

FIG. 2: Solution of the full kinetic equation (15) for $m_{\tilde{\tau}} = 200$ GeV and $m_{\tilde{G}} = 50$ GeV, corresponding to $\tau_{\rm NLSP} \approx 6\times10^6$ sec. Top: The dashed (blue) line represents the chemical potential given by Eq. (13), the solid (red) line is the solution of Eq. (15) evaluated at $x = 3$. Bottom: Chemical potential as a function of x given by Eq. (15) evaluated at $t = 5 \times 10^6$ sec (dotted blue line), $t = 10^7$ sec (dashed green line) and $t = t_{\rm dec}$ (solid red line).

accuracy of a solution of Eq. (15) for a stau lifetime longer than $\tau_{\rm NLSP} \sim 5 \times 10^8$ sec becomes questionable and untrustworthy for $\tau_{\rm NLSP} \gtrsim 10^9$ sec.

On the other hand, after freeze-out of Compton scattering, the injected energy resulting from stau decays cannot be scattered downward in frequency. But there are several other processes that could leave an imprint on the measurable CMB spectrum. For example, photons produced during stau decays have an energy much greater than the electron mass and can create electron-positron pairs through the process $\gamma + \gamma \rightarrow e^+ + e^-$. The rate of this process has a typical value of $\Gamma_{\rm DP} \approx 10^3$ sec^{-1}, provided $E_\gamma \gtrsim m_e^2/22T$ [13]. Compared to the Hubble rate $H = 1/2t$, we see that this process plays an important role in heating up the electrons. However, the raise of the electron temperature does no longer affect the CMB spectrum when Compton scattering has already frozen out.

We have also analyzed the fact that the true electron temperature $T_{e,\rm true}$ is not the same as the electron temperature T_e obtained by solving Eq. (13) due to the influence of bremsstrahlung and double-Compton scattering which reduce the chemical potential from the value $\mu_{\rm inj}$. Given the chemical potential μ at recombination time, we can calculate T_e by inserting μ into one of the equations of the system (13). We have found that $T_{e,\rm true}$ only differs from T_e by $\sim 10^{-4}$, and that changing the electron temperature in Eq. (15) by such small amounts has no effect. (This is not so surprising, as the effect is of second order.)

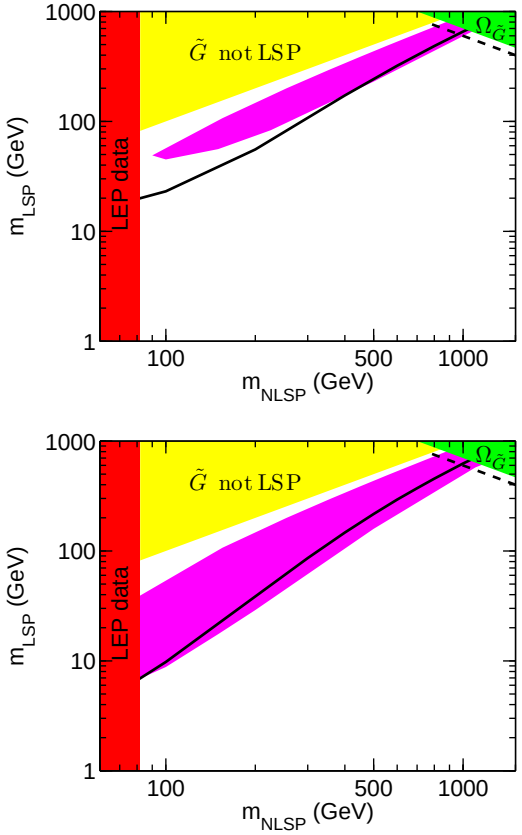

FIG. 3: Excluded and allowed regions in the $(m_{\rm NLSP}, m_{\rm LSP})$ parameter space. The light shaded region in the upper part of the graphs, labeled '$\tilde{G}$ not LSP', (yellow) is not considered since in this part of parameter space $m_{\rm NLSP} < m_{\rm LSP}$. The shaded region in the right upper corner, labeled '$\Omega_{\tilde{G}}$', (green) is excluded by the over-closure constraint $\Omega_{\tilde{G}}h^2 \lesssim 0.14$. The dark shaded region on the left, labeled 'LEP data' (red) is forbidden by LEP measurements [19]. The dashed line corresponds to $\Omega_{\tilde{G}}h^2 = 0.12$, the best fit value for the cold dark matter density from the WMAP experiment [9]. The dark shaded region in the middle (magenta) is forbidden for a chemical potential limit of $\mu < 9 \times 10^{-5}$ (top) and $\mu < 10^{-5}$ (bottom). The approximation of Ref. [5] excludes the entire region above the solid line.

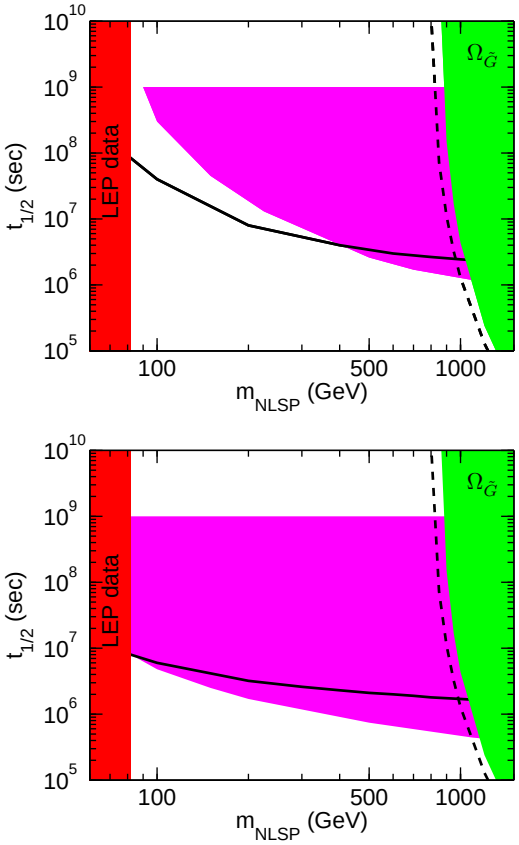

FIG. 4: Excluded and allowed regions in the $(m_{\rm NLSP}, \tau)$ plane. The dashed line corresponds to $\Omega_{\tilde{G}}h^2 = 0.12$, the best fit value for the cold dark matter density from the WMAP experiment [9]. The regions are labeled as in Fig. 3. In the top panel the limit on the chemical potential is $\mu < 9\times10^{-5}$ while we require $\mu < 10^{-5}$ in the bottom panel. The approximation of Ref. [5] excludes the entire region above the solid line.

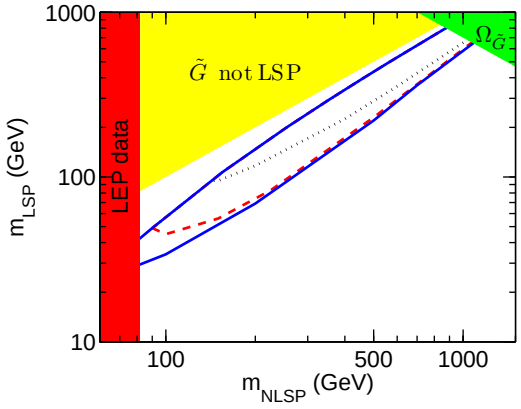

FIG. 5: Excluded and allowed regions in the $(m_{\rm NLSP}, m_{\rm LSP})$ plane for different values of the parameter ϵ and a chemical potential $\mu = 9\times10^{-5}$. The labeled regions are as in Fig. 3. The lower solid (blue) line represents the case $\epsilon = 1$, the dashed (red) line $\epsilon = 0.8$ and the dotted (black) line $\epsilon = 0.3$. The upper solid line denotes the limit on the lifetime, $\tau > 10^9$sec above which the CMB spectrum is not modified.

IV. CMB CONSTRAINTS ON THE STAU AND GRAVITINO MASSES

The FIRAS instrument aboard the COBE satellite has measured a temperature $T_0 = 2.725 \pm 0.001$ Kelvin [14], and it was able to give an upper bound for the chemical potential [1, 15], $|\mu| < 9\times10^{-5}$. This bound comes from measurements in the frequency range from 2 to 600 GHz, corresponding to $x = h\nu/T_0 \in [0.03, 10]$. There are also some measurements at lower frequencies, but their accuracy is worse, leading to a lower bound on μ which is by at least an order of magnitude higher. To obtain good accuracy in the measured interval, we numerically compute the chemical potential for $x \in [10^{-4}, 15]$. We require that the chemical potential be never higher than 9×10^{-5} within the *experimental* range $x \in [0.03, 10]$. Outside that range, μ may be larger (experiments do not rule out deviations outside the frequency range [0.5 GHz, 600 GHz]).

A point in the $(m_{\rm NLSP}, m_{\rm LSP})$-plane is considered to satisfy the CMB observational bound if the magnitude of the chemical potential never trespasses the limit 9×10^{-5} within and only within the frequency range [0.03, 10]. Due to the limitations explained in the previous section, not every point in the $(m_{\rm NLSP}, m_{\rm LSP})$-plane can be calculated, but we expect the chemical potential to be much smaller than the experimental limit for points where our calculation cannot be trusted.

An estimate of the chemical potential caused by an instantaneous energy injection is given in [5]. It is shown as a solid line in Figs. 3 to 6. This approximation is not very precise for small distortions. While it is in good agreement with our results for staus heavier than 500 GeV, it does not take account of the fact that light staus do not inject enough energy to significantly distort the spectrum. As shown in the upper panel of Fig. 3, the bound on the gravitino mass disappears for staus lighter than ≈ 100 GeV. Moreover, due to the freeze-out of Compton scattering, we have introduced a limit on the gravitino masses corresponding to a stau lifetime 10^9 sec. All gravitino masses leading to longer stau lifetimes are allowed.

Our results match quite well with the approximation given in [5] for $\mu < 10^{-5}$, as shown in the bottom panel of Fig. 3. We find the same limit for light staus and a somewhat more stringent limit for heavy staus. However, when compared to the stau lifetime (see the bottom panel of Fig.4), our numerical results give a limit on the lifetime that is up to five times shorter than the one obtained by using the approximation.

As mentioned in Sec. III A, the injected energy depends on the energy going into neutrinos. This is described by the parameter ϵ. Contrary to what is claimed in [3], our results depend significantly on this parameter. We considered the two extreme cases $\epsilon = 0.3$ and $\epsilon = 1$

and the usual case $\epsilon = 0.8$ (Fig. 5). The case $\epsilon = 0.3$ is much less constraining than $\epsilon = 0.8$, even completely disappearing for staus lighter than 140 GeV. On the other hand, the cases $\epsilon = 1$ and $\epsilon = 0.8$ match well down to $m_{\tilde{\tau}} \simeq 200$GeV below which the former becomes more stringent.

Future missions like the Absolute Radiometer for Cosmology, Astrophysics Diffuse Emission (ARCADE) [16, 17] or the Diffuse Microwave Emission Survey (DIMES) [6] experiments may improve sensitivities in the poorly studied centimeter-wavelength band, improving the limit on the chemical potential to about $|\mu| < 2 \times 10^{-6}$. In our model, if neither DIMES nor ARCADE is able to measure distortions of the CMB, gravitinos could only contribute to the missing dark matter if $\tau_{\rm NLSP} \gtrsim 10^9$ sec or $\tau_{\rm NLSP} \lesssim 2 \times 10^5$ sec (see Fig. 6). However, combining our results with other constraints [18], we find that gravitinos could not significantly contribute to the dark matter for such a bound.

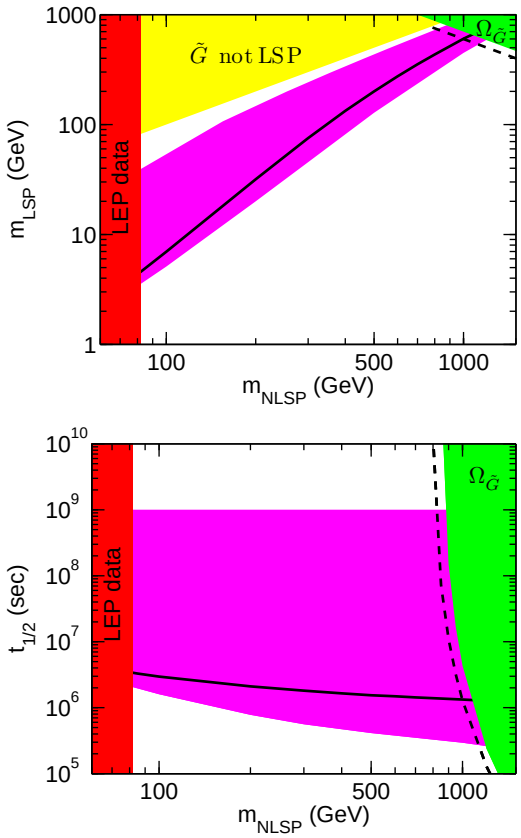

FIG. 6: Excluded and allowed regions in the $(m_{\rm NLSP}, m_{\rm LSP})$ plane (top panel) and in the $(m_{\rm NLSP}, \tau)$ plane (bottom panel) for a limit on the chemical potential of $\mu < 2 \times 10^{-6}$. The labeled regions are like in Fig. 3.

V. SUMMARY

We have studied the effect on the CMB from stau NLSP decays into gravitino LSPs, assuming that the staus freeze out with their thermal relic density. We have numerically solved the kinetic equation for the photon number density with non-instantaneous energy injection. We have found that our numerical results are in good accordance with the analytical approximation [5] for the induced chemical potential $\mu < 9 \times 10^{-5}$ if the stau is heavier than 500GeV, but differs considerably for lighter stau masses. For light staus the constraints are weaker and even disappear for $m_{\tilde{\tau}} < 100$GeV. On the other hand, the approximation underestimates the limits for stronger constraints given by $\mu < 10^{-5}$ or even more for $\mu < 2 \times 10^{-6}$. This limit, which could be achieved in planned experiments [6, 16], together with other constraints [18] would completely exclude the gravitino as dark matter candidate in models with gravity-mediated supersymmetry breaking. However, allowing a gravitino production after reheating leads to less stringent constraints than our results. We also found that the results depend sensitively on the energy injection parameter ϵ.

Acknowledgments

We are grateful to Leszek Roszkowski for many helpful remarks and to Jürg Fröhlich for discussions. We also thank Choi Ki-Young for pointing out an important error in the first version of this paper. This work is supported by the Fonds National Suisse.

[1] D. Fixsen, et al., Astrophys. J. **473**, 576 (1996).
[2] J.L. Feng, A. Rajaraman, and F. Takayama, Phys. Rev. Lett. **91**, 011302 (2003).
[3] J.L. Feng, A. Rajaraman, and F. Takayama, Phys.Rev. D **68**, 063504 (2003)
[4] L. Roszkowski and R. Riuz de Austri, JHEP **0508**, 080 (2005).
[5] W. Hu, and J. Silk, Phys. Rev. D **48**, 485 (1993).
[6] DIMES, see http://arcade.gsfc.nasa.gov/science_mu.html
[7] R.J. Scherrer, and M.S. Turner, Phys. Rev. D **33**, 1585 (1986).
[8] T. Asaka, K. Hamaguchi, and K. Suzuki, Phys. Lett. **B490**, 136 (2000).
[9] D.N. Spergel et al., Astrophys. J. Suppl. **148**, 175 (2003).

[10] M. Abramowitz, and I.A. Stegun, *Handbook of Mathematical Functions*, Dover, New York, 1972.
[11] A.P. Lightman, Astrophys. J. **244**, 392 (1981). (There is an omission of a factor 4π in the expression for bremsstrahlung).
[12] T. Padmanabhan, *Theoretical Astrophysics, Vol III*, Cambridge University Press, Cambridge 2002.
[13] M. Kawasaki, and T. Moroi, Astrophys. J. **452**, 506 (1995)
[14] J.C. Mather et al., Astrophys. J. **512**, 511 (1999).
[15] G.F. Smoot, and D. Scott in: *The Review of Particle Physics*, D.E. Groom et al., Eur. Phys. J. **C15**, 1 (2000); `astro-ph/9711069`.
[16] ARCADE, see http://arcade.gsfc.nasa.gov
[17] A. Kogut et al., ApJS, **154**, 493 (2004).
[18] J.L. Feng, and S. Su, and F. Takayama, hep-ph/0404231 (2004)
[19] Particle Data Group, http://pdg.lbl.gov